Accepted Manuscript

Pyridinium and indole orientation determines the mitochondrial uncoupling and anti-cancer efficiency of F16

Juan Xu, Huan He, Lian-Jiao Zhou, Yu-Zhu Liu, Dong-Wei Li, Feng-Lei Jiang, Yi Liu

PII: S0223-5234(18)30449-5

DOI: 10.1016/j.ejmech.2018.05.036

Reference: EJMECH 10447

To appear in: *European Journal of Medicinal Chemistry*

Received Date: 27 February 2018

Revised Date: 21 May 2018

Accepted Date: 22 May 2018

Please cite this article as: J. Xu, H. He, L.-J. Zhou, Y.-Z. Liu, D.-W. Li, F.-L. Jiang, Y. Liu, Pyridinium and indole orientation determines the mitochondrial uncoupling and anti-cancer efficiency of F16, *European Journal of Medicinal Chemistry* (2018), doi: 10.1016/j.ejmech.2018.05.036.

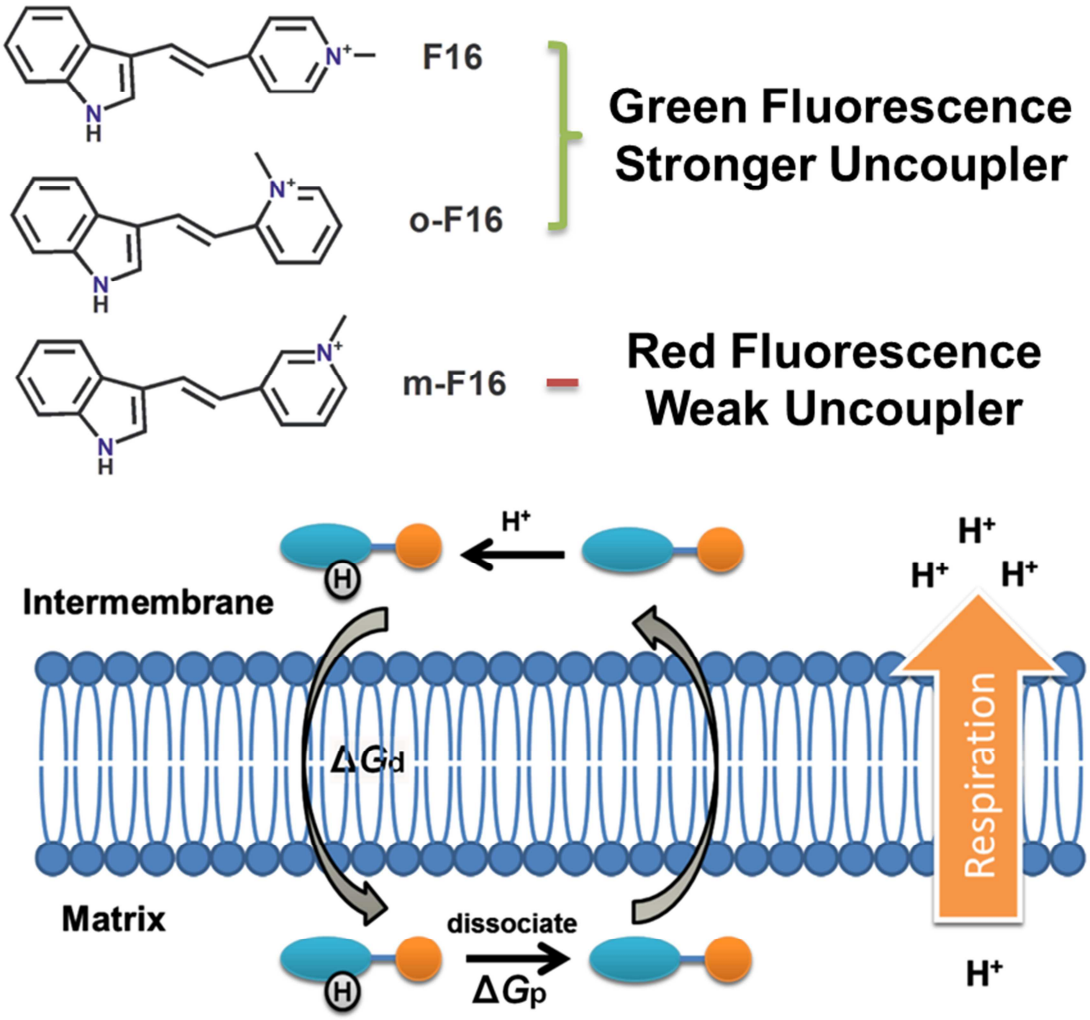

Pyridinium and indole orientation determines the mitochondrial uncoupling and anti-cancer efficiency of F16

Juan Xu[a,†], Huan He[a,†], Lian-Jiao Zhou[a], Yu-Zhu Liu[a], Dong-Wei Li[a], Feng-Lei Jiang[a,*] and Yi Liu[a,b,c,*]

[a.]State Key Laboratory of Virology & Key Laboratory of Analytical Chemistry for Biology and Medicine (MOE), College of Chemistry and Molecular Sciences, Wuhan University, Wuhan 430072, P. R. China

[b.]College of Chemistry and Material Sciences, Guangxi Teachers Education University, Nanning 530001, P. R. China

[c.]Key Laboratory of Coal Conversion and Carbon Materials of Hubei Province, College of Chemistry and Chemical Engineering, Wuhan University of Science and Technology, Wuhan 430081, P. R. China.

[†]Theses authors contribute equally to this work.

*Corresponding Author. Tel.: 86-27-68756667. Fax: 86-27-68754067. Email address: yiliuchem@whu.edu.cn, fljiang@whu.edu.cn.

Abstract F16 is a mitochondria-targeted, broad-spectrum anticancer agent in the pre-clinic cancer therapy. Here we developed two fluorescent isomers of F16 (o-F16 and m-F16) with entirely different photophysical properties, uncoupling activity, and cytotoxicity by merely modifying the linking orientation of pyridinium and indole units. Individually, o-F16 acted as a strong uncoupler to reduce the mitochondrial respiration efficiency, while m-F16 could hardly uncouple the mitochondrial respiration due to its poor proton dissociation capability. Owing to their intrinsic fluorescence, o-F16 and m-F16 could specifically image mitochondria in the green and red channel, respectively. This work could provide useful information for the development of uncouplers and design of mitochondrial-targeted drugs.

Introduction

Mitochondria have long been considered as the cell's growth energy factory[1]. Recent studies reveal that mitochondria also play an essential role in the control of cell death[2]. Compared with normal cells, mitochondria in cancer cells exhibit lower oxidative phosphorylation, higher trans-membrane potential, increased reactive oxygen species (ROS) and deregulated mitochondrial apoptotic pathway[3]. These features make mitochondrial-targeted anticancer drugs a very promising strategy for the malignancy treatments[3, 4].

F16 (Scheme 1) is a kind of delocalized lipophilic cations (DLC) screened from approximately 16,000 small molecules[5]. F16 selectively accumulates in mitochondrial matrix driven by the negative transmembrane potential and induces a strong inhibition of tumour growth[6]. Our previous studies indicated that the F16-triggered cell death was closely associated with its uncoupling effect on mitochondrial respiration[7]. Treatment of cancer cells with F16 resulted in a significant decrease in intracellular ATP level and subsequent energetic breakdown. These features suggested that F16 may serve as an uncoupler on mitochondria. We have also previous proved that F16 could be utilized as a targeting moiety for selective delivering of fluorescent probes[8] or anticancer drugs[9] into mitochondria. Based on our investigations, F16 could act as a promising fluorescent and toxic substitute for the most commonly used tetraphenylphosphonium (TPP)[10,11,12]. However, there still exists room for improving the biological activities of F16 such as fluorescence and toxicity. This requires a detailed investigation on the structure-activity relationship (SAR) of F16. For example, it has been reported that incorporation of fluorine on indole ring of F16 could enhance its cellular uptake and cytotoxicity[13]. In this work, we developed two fluorescent F16 isomers (o-F16 and m-F16, Scheme 1) by simply modifying the linking orientation of pyridinium and indole moiety. Cellular and sub-cellular investigations suggested the two isomers

significantly varied in fluorescence and toxicity.

Experimental

Chemicals and reagents Gramine, para-pyridnecarboxaldehyde, rhodamine123 (Rh123), dinitrophenol (DNP), carbonyl cyanide p-trifluo-methoxyphenylhydrazone (FCCP), 2,7-dichlorfluorescein diacetate (DCFH-DA), 5,5‘,6,6‘-Tetrachloro-1,1‘,3,3‘-tetraethyl-imidacarbocyanine iodide (JC-1) and rotenone were obtained from Sigma Aldrich (St. Louis, USA). 3-(4, 5-dimethylthiazol-2-yl)-2, 5-diphenyltetrazolium bromide (MTT) was obtained from Amresco (Solon, USA). Dulbecco’s modified Eagle’s medium (DMEM) and fetal bovine serum (FBS) were purchased from Gibco (MA, USA). Modified DMEM (no Glucose) were purchased from Thermofisher Scientific (MA, USA). Annexin V-PE/7-AAD apoptosis kit was purchased from MultiSciences (Hangzhou, China). Tyrpsin-EDTA solution was purchased from Beyotime Technology (Shanghai, China). Antibodies were purchased from Cell Signaling Technology (Boston, USA). All other common reagents were of analytical reagent grade from Shenshi (Wuhan, China) and used without further purification.

Synthesis A mixture of para-pyridnecarboxaldehyde (0.30 mL, 3.0 mmol), N-butyl phosphorus (0.74 mL, 3.0 mmol), gramine (348 mg, 2.0 mmol), and 5.0 mL acetonitrile was stirred at 80 °C for 24 h. The mixture

was concentrated under vacuum, and the oil product was purified by silica chromatography with hexanes/EtOAc (1:1 V/V) to give non-charged precursor (yield 42.5%) for F16. The non-charged precursor (10 mg, 0.54 mmol) were added to 3 mL dry DMF at room temperature and stirred overnight. DMF was removed and the residues were recrystallized in $CHCl_3$ (0.3 mL) and n-hexane to obtain F16 (9.74 mg, yield 51.7%). 1H NMR (400 MHz, DMSO-d6): δ=4.169 (s, 3H), 7.250-7.266 (m, 2H), 7.318(s, 1H), 7.526 (d, 1H),7.963(s, 1H), 8.110-8.126(m, 2H), 8.133-8.258(m, 2H), 8.669-8.691(d, 2H), 11.939(s, 1H); ESI-MS (m/z): calcd: 235; found: 235.2. o-F16 and m-F16 were synthesized from ortho- or meta- pyridnecarboxaldehyde using the same method. The yields were 35.0% and 54.3%, respectively. 1H NMR for o-F16 (400 MHz, DMSO-d6): δ=4.336 (s, 3H), 7.223-7.518 (m, 3H), 7.540 (d, 1H), 7.772(s, 1H), 8.110-8.113(m, 2H), 8.245-8.386(m, 2H), 8.523(d, 1H), 8.770 (d, 1H), 12.041(s, 1H); ESI-MS (m/z): calcd: 235; found: 235.2. 1H NMR for m-F16 (400 MHz, DMSO-d6): δ=4.334 (s, 3H), 7.187-7.237 (m, 3H), 7.449 (d, 1H),7.885(s, 1H), 8.040-8.092(m, 2H), 8.688-8.711(d, 2H), 9.208(s, 1H), 12.041(s, 1H); ESI-MS (m/z): calcd: 235; found: 235.2.

Cytotoxicity assay Human gastric carcinoma (SGC-7901) cells, human breast adenocarcinoma cells (MCF-7) and human alveolar basal epithelial cells (A549) were cultured in DMEM medium containing 10% fetal

bovine serum (FBS, Gibco) in a humidified atmosphere containing 5% CO_2 at 37 °C. The cells were seeded onto 96-well plates at 10^4 cells per well and incubated for 24 h. F16 isomers with varying concentrations were respectively added to the cells followed by further culture of 24h or 48h, and the culture media were discarded. MTT solutions in PBS were added to each well followed by incubation for 4 h. The supernatant was discarded and 150 μL DMSO was added into each well. The absorbance value at 570 nm at each well was recorded by a microplate reader. The survival curves plotted as a function of the concentration of F16 isomers and cell viability rate (%).

Confocal laser scanning microscopy measurements SGC-7901 cells were seeded onto 35 mm dishes and incubated for 24 h for attachment. Cells were then treated with o-F16 or m-F16 (10 μM) for 4 h. Mitotracker Red (0.2 μM) or Mitotracker Green (0.2 μM) were used to stain the cells for 30 min. The cells were then examined by confocal laser scanning microscopy. Fluorescence images were obtained by a PerkinElmer UltraVIEW VoX confocal system. The 488 laser was used to excite o-F16 or Mitotracker Green, m-F16, and o-F16, and 561 laser was used to excite Mitotracker Red. The fluorescence emission signals were separated by using a 525/25 nm filter (green channel) and a 605/20 nm filter (red channel), respectively.

Measurement of mitochondrial membrane potential The SGC-7901

cells were seeded onto 6-well plates overnight. After incubation with F16 isomers (1.0 and 5.0 μM) for 4h, stained with JC-1 for 1 h. FCCP (2.0 μM) was set as positive control. The cells were washed 3 times with PBS, dissociated with tyrpsin-EDTA solution, resuspended in PBS, then analyzed with BD ACCURI C6 flow cytometer by detecting the fluorescence of JC-1 at channel 1 and 2.

Determination of intracellular ATP The SGC-7901 cells were grown in DMEM medium without or with F16 isomers (5.0 μM) for 48 h. Intracellular ATP levels were determined by a luciferin-luciferase method[7]. Then the cells were harvested and lysed according to the manufacturer's procedure. The intracellular ATP level in SGC-7901 cells cultured in glucose-free DMEM medium (supplemented with 10 mM D-galactose) was also determined using the same method.

Annexin V-PE/7-AAD double staining assay SGC-7901 cells were incubated in DMEM medium with 5.0 μM of F16, m-F16 or o-F16 for 48 h. Then the cells were harvested, centrifugated, and resuspended in 500 μL staining buffer containing both Annexin V-PE and 7-AAD, to a final concentration of 50 nM. After 10 min, the cells were analyzed with BD ACCURI C6 flow cytometer to record the fluorescence in channel 3 and 4.

Western blot analysis SGC-7901 cells were treated with F16 isomers for 24h. The whole cell pellets were then lysed with RIPA lysis and

extraction buffer (25 mM Tris·HCl, 150 mM NaCl, 1% NP-40, 1% sodium deoxycholate, 1% SDS, pH=7.6) for 30 min. After 13000 rpm centrifugation for 10 min, the supernatant was determined by BCA protein assay kit (Beyotime, Wuhan, China). An equal amount of the total protein was loaded onto an SDS-PAGE minigel and electro-transffered onto PVDF membranes. Proteins were detected using primary antibodies, followed by HRP-conjugated secondary antibody and visualized using ECL substrate. Immunoblot quantification was performed by ImageJ software.

Isolation of rat liver mitochondria Wistar rats (200-250 g) were purchased from Hubei Research Centre of Experimental Animals (Wuhan, China). Rat liver mitochondria were isolated by standard differential centrifugation[14]. The concentration of mitochondria protein was measured by the Biuret method. All operations were performed at 0-4 ºC.

Measurement of mitochondrial respiration Mitochondrial respiration rates of isolated mitochondria were measured with a Clark-type oxygen electrode in a 1 mL thermostated, water-jacketed, closed chamber with magnetic stirring. Mitochondria (1 mg/protein) were incubated in 1 mL medium containing 250 mM sucrose, 20 mM KCl, 5 mM K_2HPO4, 10 mM HEPES, and 2 mM $MgCl_2$, 1 μM rotenone, for 3 min before energization with 5 mM succinate (state 4). State 3 respiration were initiated by adding ADP (100 μM).

Measurement of mitochondrial membrane potential of isolated liver mitochondria Changes in mitochondrial membrane potential ($\Delta\Psi_m$) of isolated liver mitochondria were indicated by the accumulation of Rh123 (250 μM) as monitored by the changes in fluorescence emission intensity at 25 ºC (λ_{ex} = 488 nm, λ_{em} = 525 nm)[15].

Measurement of mitochondrial H^+ permeabilization Mitochondrial swelling was measured spectrophotometrically by monitoring the absorbance at 540 nm over 10 min at 25 ºC by UNICO 4802 UV-Vis Double Beam Spectrophotometer. Mitochondria were suspended in 2 mL buffer containing 135 mM K-acetate, 5 mM HEPES, 0.1 mM EGTA, 0.2 mM EDTA and 2 μM rotenone.

Measurement of mitochondrial membrane fluidity Mitochondrial membrane fluidity was measured by the fluorescence anisotropy changes of hematoporphyrin (HP)-labeled mitochondria at 626 nm (λ_{ex} = 520 nm) by an LS-55 fluorophotometer (Perkin-Elmer, Norwalk, CT).

Observation of mitochondrial ultrastructure Observations of mitochondrial ultrastructure were performed with a JEM-100CX II transmission electron microscope (JEOL, Tokyo, Japan). Mitochondria were incubated in the presence of 50 μM of F16, o-F16 or m-F16 at 25 ºC for 30 min, and then fixed for 30 min at 4 ºC using glutaraldehyde at a final concentration of 2.5% (v/v) in PBS buffer, then the micropellets were postfixed with 1% (w/v) osmium tetroxide and dehydrated.

Molecular dynamics simulations We used NAMD 2.6 for running MD simulations[15] and the Adaptive Biasing Force (ABF) method for modeling the potentials of mean force (PMF). The temperature was maintained with the Berendsen thermostat[16] using a coupling parameter of 5 ps^{-1}. The pressure was maintained at 1 atm by the Langevin piston method[17] with piston mass of 100 atomic mass unit and Langevin collision frequency of 50 ps^{-1}. Non-bond interactions were computed using the particle mesh Ewald method with 10 Å cutoff for the electrostatic interactions and the switching function between 10 and 12 Å for the van der Walls interactions. The non-bond interaction list was constructed using a cutoff of 14 Å, update every 50 steps. The covalent bonds involving hydrogen atoms were constrained using the SHAKE algorithm. MD integration step size was set to 2 fs.

Molecular structure of hydrated palmitoyloleylphosphocholine (POPC) bilayer was constructed In VMD software[18]. The hydrated POPC bilayer consisted of 100 lipid unit with an aqueous phase surrounded by 5450 water molecules. The system was large enough to ensure that the F16 isomers in the middle of the membrane did not perturb the entire membrane structure. Molecular force field parameterization for F16 isomers was obtained by the combination of the standard CHARMM27 parameters with parameters determined by ab initio calculations using the GAUSSIAN 09 program. The equilibrium bond lengths and angles were

obtained from DFT calculations with B3LYP functional and Pople 6-31G(d) basis set. Partial charges of atoms were calculated by electrostatic potential fitting. At the starting conformation, the F16 molecule (or o-F16, m-F16) was 25 Å away from the upper of the lipid membrane.

MD simulations were performed in the NPT ensemble at T = 320 K and pressure 1 atm. After initial 25 ns equilibration, the ABF calculations in the NAMD implementation were initiated by dragging the N atom on pyridine moiety from the bulk toward the positive half of the z-axis toward the bilayer. The dragging force was determined within the classical thermodynamic integration formalism. The free energy derivative was estimated locally as the simulation progresses, thereby providing a continuous update of the biasing force. When applied to the system, this bias generates a Hamiltonian exempt of a net average force along z. MD simulations for each F16 isomer continued for 160 ns.

Results and Discussion

F16, o-F16, and m-F16 were first synthesized in two steps from gramine and para-, ortho- or meta-pyridinecarboxaldehyde, respectively (Scheme 1). The absorption and emission spectra of the three compounds are shown in Fig. S1. Surprisingly, these isomers were entirely different in absorption and emission spectra despite their high similarity in

chemical structures. F16 and o-F16 gave green fluorescence with emission maxima at 523 and 509 nm respectively, while m-F16 gave red fluorescence with an emission maximum at 602 nm. The difference in emission maximum of m-F16 came from its significant lower energy gap between HOMO and LUMO (Fig. S1c). Especially, the configuration of LUMO of m-F16 was entirely different from F16 and m-F16, while their HOMO configurations were similar.

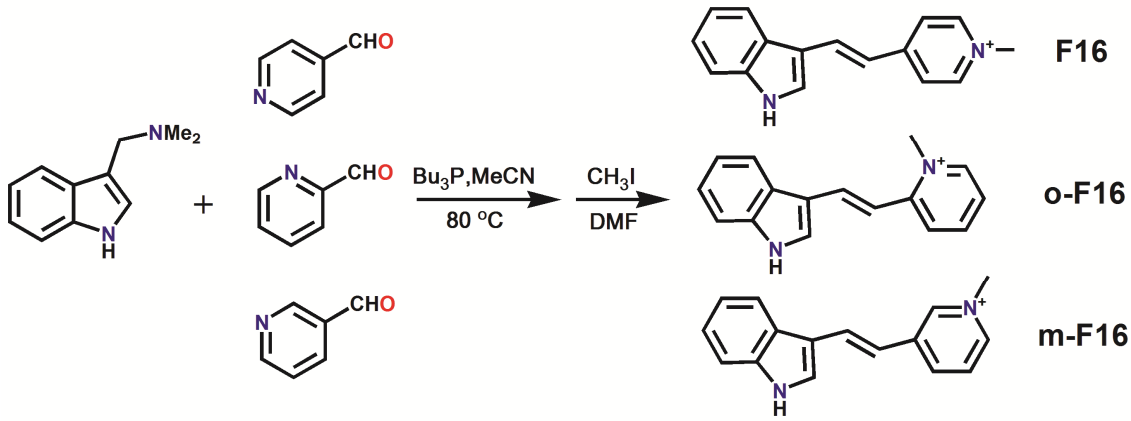

Scheme 1 Synthetic route of F16, o-F16 and m-F16.

We then turned to investigate the subcellular localization of o-F16 and m-F16 in human gastric carcinoma (SGC-7903) cell line by their intrinsic fluorescence. Cells were incubated with 10 μM of o-F16 or m-F16 for 4 hours, and confocal microscopic imaging experiments were then conducted as shown in Fig. 1 and Fig. S3. It can be observed that the green fluorescence of o-F16 was perfectly overlapped with the red fluorescence of Mito Tracker Red (Pearson's Correlation = 0.943), while the red fluorescence of m-F16 was perfectly overlapped with the green

fluorescence of Mito Tracker Green (Pearson's Correlation = 0.970), indicating that both of o-F16 and m-F16 could be accumulated in mitochondria of SGC-7901 cells. This might arise from the excellent dispersity of positive charge of the three compounds (Fig. S2). To preclude cell line-specific artifacts, localization experiment was also performed on human breast adenocarcinoma cell line (Fig. S4).

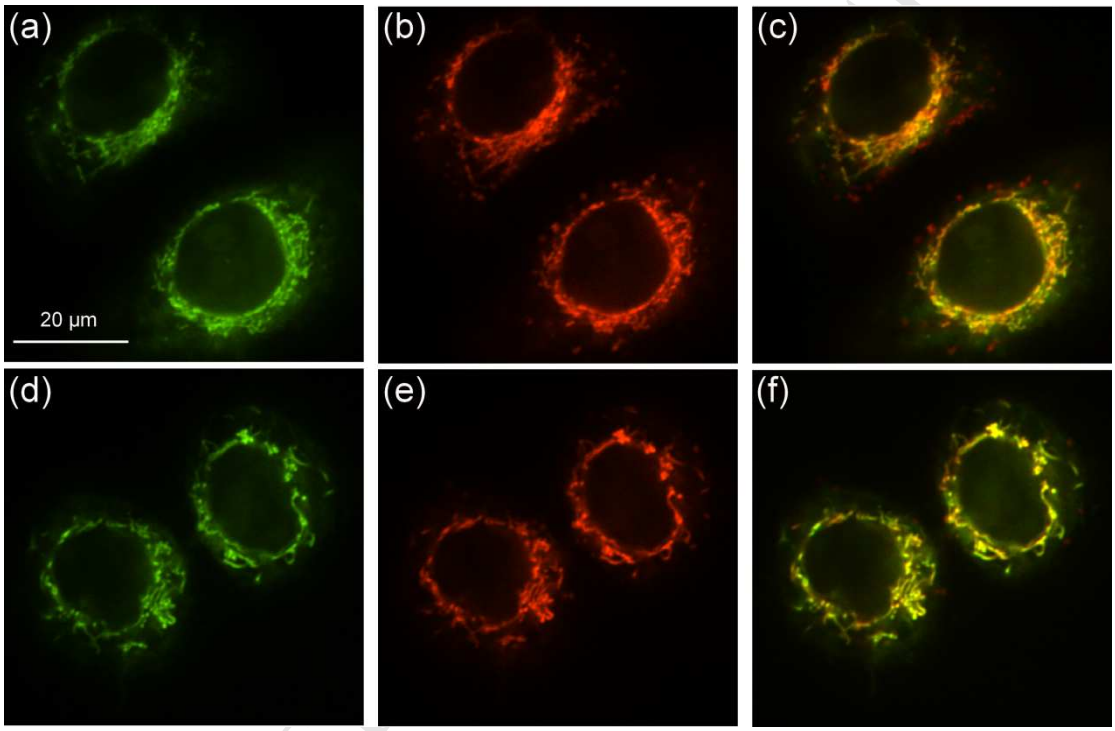

Fig. 1 Confocal fluorescence imaging of o-F16 (a-c) and m-F16 (d-e) in SGC-7901 cells. (a) Fluorescent image of o-F16 in SGC-7901 cells (10 μM, λ_{ex} = 488 nm. (b) Fluorescent image of Mitotracker Red (0.2 μM, λ_{ex} = 561 nm). (c) Merged image of a and b. (d) Fluorescent image of Mitotracker Green (0.2 μM, λ_{ex} = 488 nm). (e) Fluorescent image of o-F16 (10 μM, λ_{ex} = 488 nm). (f) Merged images of d and e. The inserted bar indicates 20 μm.

The cytotoxicity of the three compounds against three different tumor cell lines were then investigated by a standard MTT [(3-(4, 5)-dimethylthiazol)-2,5-diphenyltetrazolium bromide] method (Fig. 2a, Table S1). In agreement with previous reports, F16 isomers displayed strong cytotoxicity on SGC-7901 cells (IC_{50} = 3.5 ± 0.3 μM). However, the cases were entirely different for its two isomers. As shown in Fig. 2a, o-F16 exhibited inhibitory effects on viability and growth of SGC-7901 cells (IC_{50} = 5.7 ± 0.7 μM), while the inhibition effects of m-F16 (IC_{50} > 50 μM) were feeble. The inhibition rate of SGC-7901 cells treated with 20 μM of m-F16 was less than 15%. We further investigated the effects of the three compounds on the physiological properties of mitochondria. Changes in mitochondrial membrane potential $\Delta\Psi_m$ were indicated by the ratio of red and green fluorescence of JC-1[19]. We can observe that F16 and o-F16 significantly induced the dissipation of $\Delta\Psi_m$ after 4 h incubation, while the apoptosis of the cell has not been initiated (Fig. S5) The effect of m-F16 on $\Delta\Psi_m$ dissipation was very insufficient. In mitochondria, ATP synthesis was closely related to $\Delta\Psi_m$. As shown in Fig. 2c, the intracellular level of ATP in SGC-7901 cells decreased about 47.2%, 42.1% and 5.1% after the treatment of 5 μM F16, o-F16 and m-F16. The results of $\Delta\Psi_m$ dissipation and ATP synthesis blockage indicated that m-F16 was less mitochondriotoxic than F16 and o-F16. The strong inhibition effects of F16 and o-F16 on mitochondria finally

resulted in apoptosis in SGC-7901 cells, as revealed by a typical Annexin V-PE/7-AAD double staining assay[20], while the effect of m-F16 on apoptosis was not significant.

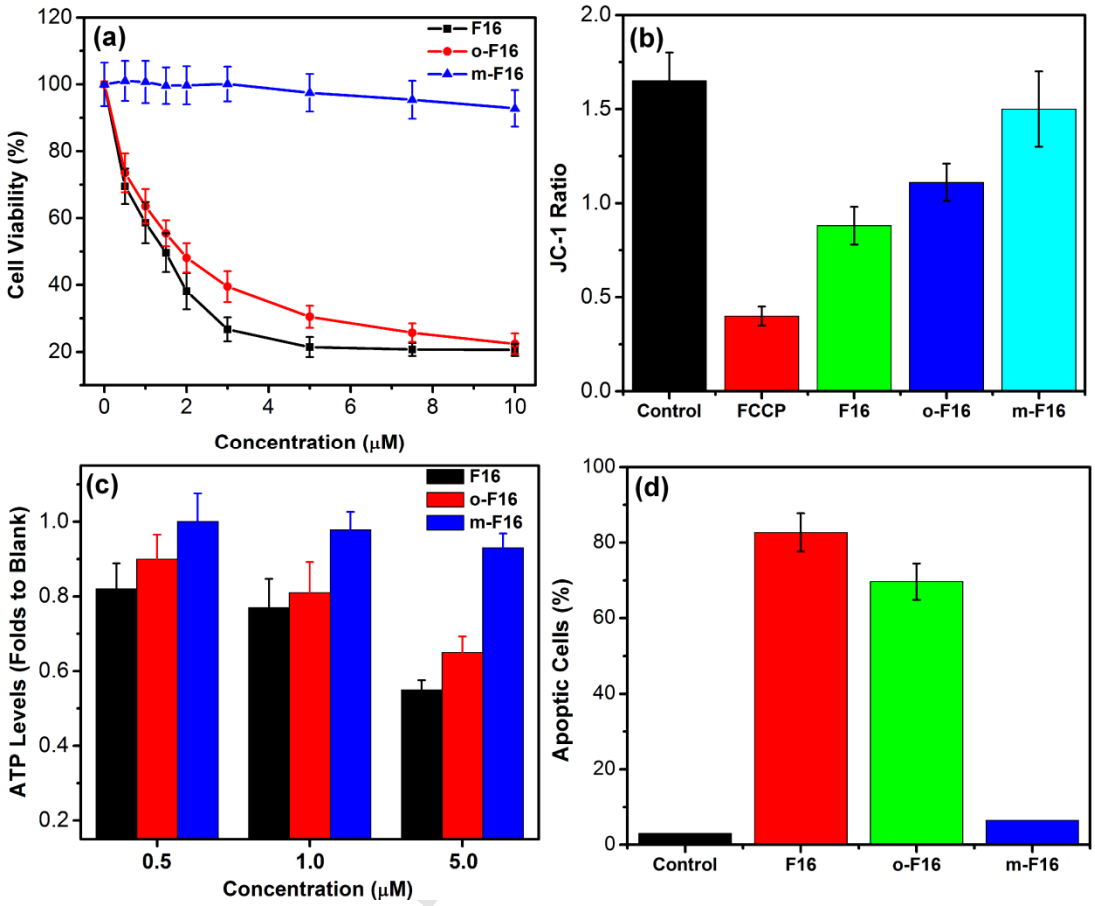

Fig. 2 (a) Cell viability of SGC-7901 cells incubated with different dosage of F16 isomers for 48h. (b) The collapse of mitochondrial membrane potential ($\Delta\Psi_m$). SGC-7901 cells were incubated with F16 isomers for 4h, followed by JC-1 staining. The JC-1 red/green ratios are presented as mean ± SD of three independent samples. Greater red/green ratio values reflect more polarized $\Delta\Psi_m$. (c) The change of intracellular ATP level. SGC-7901 cells were treated with F16 isomers for 48h, and ATP level was determined. (d) The results of apoptosis of SGC-7901 cells

by Annexin-PE/7-AAD double staining assay. Cells were treated by F16 isomers (5.0 μM) for 48h. Experiments were all performed in three replicates, and the error bars represent standard deviations.

Cells cultured in DMEM medium could compensate for the loss of mitochondrial ATP by glycolysis. The intracellular ATP and apoptosis assay was also conducted on SGC-7901 cells incubated in glucose-free medium containing 10 mM galactose. As shown in Fig. S6, we can find the ATP level significantly decreased after the addition of F16 isomers in galactose supplemented medium. Notably, m-F16, which could hardly impair the ATP production in glucose-containing medium, reduce the ATP level by ~42%. The percentage of apoptosis cells also increased as the ATP amount decreased.

To character the apoptotic pathways involved in o-F16 and m-F16 induced lethality, we determined the expression level of Bcl-2 and Bax, two critical apoptosis-related proteins localized to the outer membrane of mitochondria. As shown in Fig. 3, o-F16 up-regulated Bcl-2 and down-regulated Bax, while the effect of m-F16 was relatively weaker. These results supported o-F16 and F16 induced cell death in mitochondrial apoptosis pathway. As Caspase3 is known as the apoptotic executor, we also monitored the expression level of cleaved-Caspase3. We observed that o-F16 significant increased the expressions of

cleaved-Caspase3, while the effects of m-F16 were minor. These results were in good agreements with the cell death experiments.

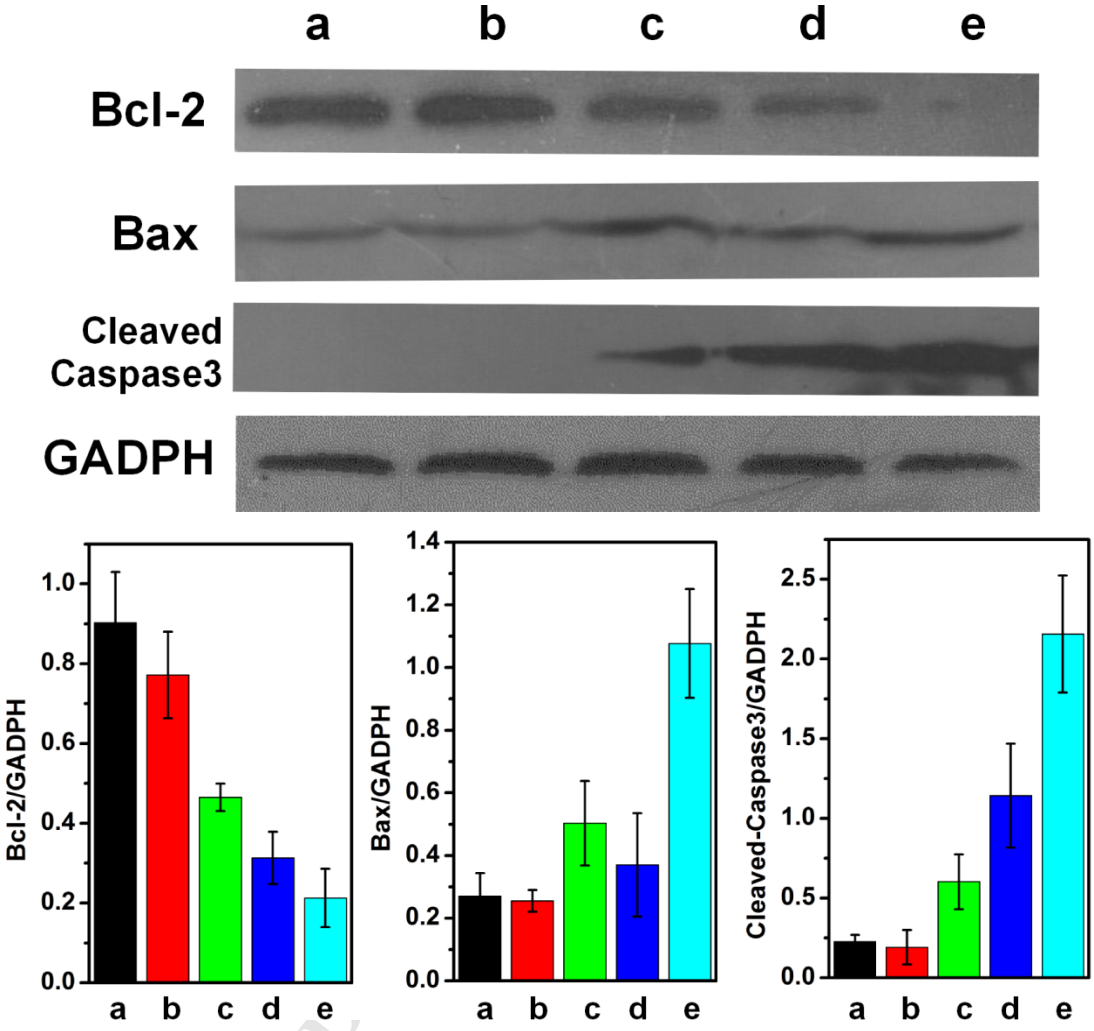

Fig. 3 F16 isomers induce apoptosis through regulation of Bcl-2/Bax and activation of Caspase3. After treatment with m-F16 and o-F16 for 48h, the expression level of Bcl-2, Bax, and cleaved-Caspase3 were determined by western blot analysis. GADPH was measured as a loading control. a, control; b, 1 μM m-F16; c, 5 μM m-F16; d, 1 μM o-F16; e, 5 μM o-F16. Experiments were all performed in three replicates, and the error bars represent standard deviations.

The substantial effects on $\Delta\Psi_m$ collapse and ATP degradation indicated that F16 and o-F16 might act as a mitochondrial uncoupler[21]. Isolated mitochondria have been validated as an efficient model to investigate the direct toxic effects of mitochondrial-targeted drugs or poisons[22, 23]. Rat liver mitochondria were isolated by differential centrifugation method as previously described[22]. It has to be mentioned that there exist differences between mitochondria of cancerous and non-cancerous tissue, but the isolated mitochondrial could serve as useful tools for the investigation of mitochondrial respiration and uncoupling. Effects of the three compounds on respiration of isolated mitochondria were measured using a standard polarographic technique with a Clark-type oxygen electrode. As shown in Fig. 4a, the state 3 (ADP-stimulated) respiration rates were slightly reduced with the addition of F16, o-F16 or m-F16, while the state 4 (non ADP-stimulated) respiration increased in a dose-dependent manner. At a concentration of 50 μM, the state 4 respiration rates of mitochondria treated with F16 and o-F16 increased about two folds, while that of m-F16 increased about 50%. These results indicated that F16 and o-F16 induced a stronger uncoupling effect than m-F16. The efficiency of oxidative phosphorylation was assessed in Fig. 4b by calculating the respiratory control ratio[24] (RCR), defined as the rate of state 3 and state 4 respiration. We can find in Fig. 4b that the respiration efficiency decreased after treatment of F16 isomers. Notably, the uncoupling

efficiency of F16 and o-F16 at 50 μM was equivalent to 2, 4-dinitrophenol (DNP) at the same concentration, which was widely regarded as a strong mitochondrial uncoupler.

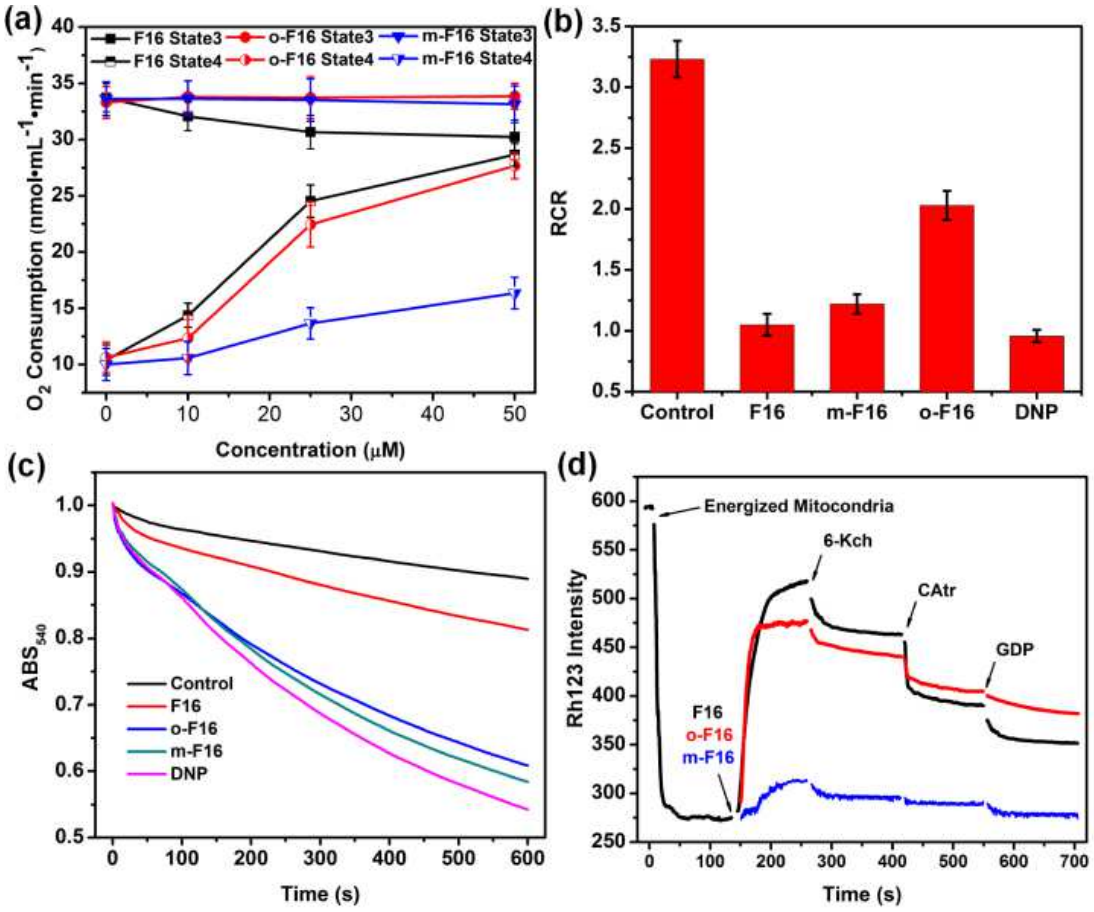

Fig. 4 Uncoupling effects of F16, o-F16 and m-F16. (a) Effects of F16 isomers on state 3 and 4 respiration rates. The O_2 consumption represents the averaged consumption speed in incubation time of 5 minutes, and error bars represent standard deviations. (b) Effects on respiration control ratio (RCR) at a concentration of 50 μM. DNP (50 μM) was used as a positive control. (c) F16 isomers (50 μM) increased the IMM permeation to H^+. IMM permeation to H^+ was monitored by the 540 nm absorbance of mitochondrial suspension in medium containing K-Acetate. (d)

375 Protective effects of 6-Kch, CAtr, and GDP on F16 induced
376 mitochondrial membrane potential ($\Delta\Psi_m$) collapse. $\Delta\Psi_m$ was recorded by
377 the fluorescence intensity of Rh123.
378
379 To further examine the mechanism for uncoupling action of F16
380 isomers, we investigated their effects on mitochondrial swelling in
381 hyperosmotic potassium acetate medium[25]. Protonated acetate can cross
382 the mitochondrial inner membrane (MIM) and dissociate to acetate anion
383 and H^+, producing a proton gradient. Matrix swelling occurred when the
384 proton gradient was dissipated. We can find in Fig. 4c that absorbance
385 decreased rapidly in the presence of F16 isomers, indicating a quick
386 dissipation on proton gradient across the MIM. These result represented
387 that the three compounds induced the proton leak from the mitochondrial
388 matrix into the inter-membrane space, that is to say, F16 and its two
389 isomers acted as protonophores to affect the respiration[14]. The direct
390 influence of uncoupling of mitochondrial respiration induced by F16 and
391 o-F16 was the collapse of $\Delta\Psi_m$ (Fig. 4d), as indicated by the increase of
392 fluorescence intensity of Rhodamine 123[15] (Rh123). In accordance with
393 the measurement in SGC-7901 cells, the $\Delta\Psi_m$ collapse induced by m-F16
394 was significantly weaker than F16 and o-F16. The dissipation in $\Delta\Psi_m$
395 induced by F16 isomers could be partially reserved by the adding of
396 6-ketocholestanol (recoupler for FCCP), CAtr (an inhibitor of adenine

nucleotide translocator) and GDP (an inhibitor for uncoupling proteins), indicating the uncoupling effects of the three isomers were related with various transporters located in the MIM[16].

Recent studies have reported that dissipation of $\Delta\Psi_m$ was always accompanied by the occurrence of mitochondrial membrane permeation transition (MPT)[29]. We then turned to investigate the effects of F16 isomers on MPT from the observation of mitochondrial ultrastructure. As shown in Fig. 5(a), mitochondrial extracted from rat liver maintained their integrity, with classical ultrastructure containing well defined outer membrane, narrow intermembrane space, and dense cristae. After incubation with F16 (b) and o-F16 (c) for 30 minutes, an increase of mitochondrial volume was observed, this indicated that mitochondrial swelling occurred. The mitochondria appeared to maintain a globular configuration with decreased matrix electron density, clustered cristae, enlarged intermembrane space and expanded volume, which was the most direct evidence of membrane permeability transition (MPT) occurrence. As for m-F16 (Fig. 5d), no visible matrix swelling was observed. In good agreement with its weaker uncoupling activity, effects of m-F16 on structure and function of mitochondria was minor, which could be revealed from the monitoring of matrix swelling (Fig. S7) and measurement of inner membrane fluidity (Fig. S8).

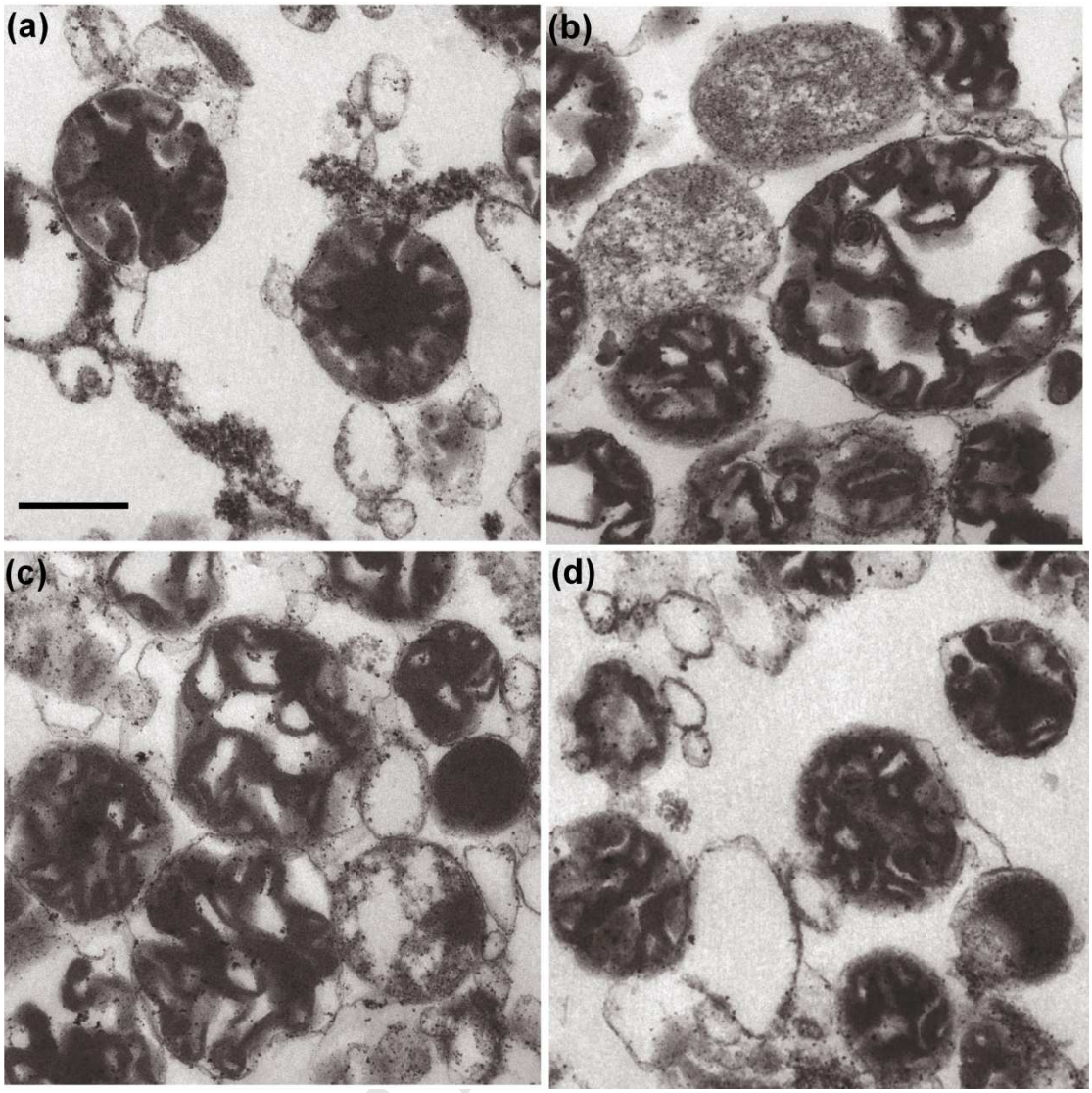

Fig. 5 Effects of F16 isomers on mitochondrial ultrastructure observed by the transmission electron microscopy (TEM). (a) Fresh liver mitochondrial were incubated in medium containing 200 mM sucrose, 10 mM Tris, 10 mM Mops, 1 mM Na_3PO_4, 10 μM EGTA-Tris, 0.5 μg/mL oligomycin, 5 mM succinate and 2 μM rotenone; pH = 7.4. (b) Mitochondria were incubated in the same medium with the addition of 50 μM F16 for 30 min. (c) 50 μM o-F16 for 30 min. (d) 50 μM m-F16 for 30 min. The inserted bar represents 0.5 μm.

We then turned to investigate the reason for the discrepancy in uncoupling efficiency of the three compounds. It has been widely accepted that the uncoupling activity for an uncoupler was determined by its proton dissociation capability and translocation barrier across the MIM[16] (Fig. 6a). Molecular dynamic (MD) simulations approach was then applied to stimulate the movement of F16 isomers through a bilayer planar phospholipid membrane[30] (BLM). Adaptive biasing force (ABF) was applied to the nitrogen atom on pyridine moiety. The free energy profile was constructed by integrating the mean force applied to the molecule along the membrane plane. We can find in Fig. 6b that the transmembrane barriers (ΔG_p) for F16 isomers were very low due to their planar and hydrophilic molecular structure. More importantly, the transmembrane barrier for the three isomers was very similar in value. The capability of the three compounds to dissociate proton was also investigated by theoretic methods. The total energy of F16 isomers ($E_{pronated}$) and their dissociated forms ($E_{dissociated}$) were calculated using density functional theory (DFT) method with 6-31*G*(d) basis set. The dissociation energies[31] (ΔG_d) for F16 or its isomers were then calculated as ($E_{pronated}$ - $E_{dissociated}$). As shown in Fig. 6c, we can observe that the dissociation energy for m-F16 was relatively higher than that of F16 and o-F16, indicating m-F16 was more difficult to dissociate proton. The difference in proton dissociation cloud also be reflected from the

measurement of dissociation constant (pK_a) for the compounds. In the cellular mitochondrial matrix, the pH was in the range of 7.8 to 8.1 depending on the cell types[32]. The high pK_a value for m-F16 (pK_a = 8.83) than F16 and o-F16 (7.96 and 8.15, respectively) indicated that m-F16 might be difficult to dissociate protons in the mitochondrial matrix. These results were in good agreements with the significant lower uncoupling efficiency.

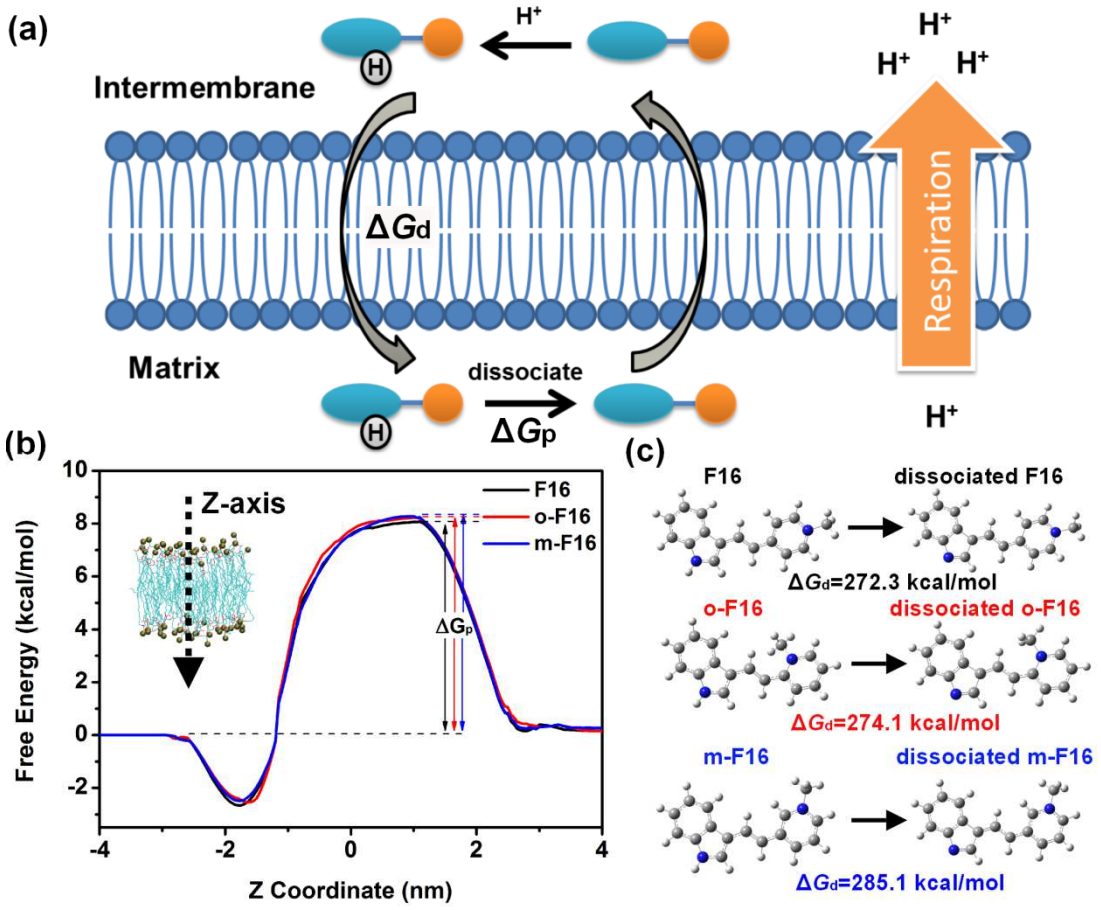

Fig. 6 (a) Scheme of F16 isomers-mediated proton transport across the MIM. (b) Free energy profiles of F16 isomers translocation across the membrane calculated from MD simulations. (c) Dissociation energies for F16 isomers.

Conclusion

In conclusion, we presented here two isomers of F16 (o-F16 and m-F16) with different fluorescence by merely modifying the linking orientation of pyridinium and indole. Fluorescent images of live cells and MD simulations indicated the two isomers could readily diffuse across the biomembranes and accumulate into mitochondria. Toxicological data on SGC-7901 cell and isolated mitochondria indicated that o-F16 acted as a strong uncoupler to reduce the respiration efficiency and subsequently induced mitochondrial membrane permeation transition and cellular apoptosis. Differently, m-F16 could hardly uncouple the mitochondrial respiration due to its poor proton dissociation capability. Importantly, m-F16 was red-emitting and low toxic, making it a very promising fluorescent substitute for TPP to delivery specific probes or sensors into mitochondria. This work may open a new door for the development of mitochondrial uncouplers and design of novel mitochondrial-targeted drugs.

Conflicts of interest

There are no conflicts to declare.

Acknowledgements

This work was supported by the National Natural Science Foundation of China (21673166, 21473125), Guangxi Science and Technology Project (GuiKeAD17195081), and Bagui Scholar Program of Guangxi Province (2016).

References

1 N. Raimundo, *Trends Mol. Med*., 2014, **20**, 282-292.

2 S. W. Tait and D. R. Green, *Nat. Rev. Mol. Cell Biol.*, 2010, **11**, 621-632.

3 S. Fulda, L. Galluzzi and G. Kroemer, *Nat. Rev. Drug Discov.*, 2010, **9**, 447-464.

4 A. Wongrakpanich, S. M. Geary, M. L. Joiner, M. E. Anderson and A. K. Salem, *Nanomedicine*, 2014, **9**, 2531-2543.

5 V. R. Fantin, M. J. Berardi, L. Scorrano, S. J. Korsmeyer and P. Leder, *Cancer Cell*, 2002, **2**, 29-42.

6 V. R. Fantin and P. Leder, *Cancer Res.*, 2004, **64**, 329-336.

7 J. Wang, H. He, C. Xiang, X. Yang Fan, L. Y. Yang, L. Yuan, F. L. Jiang and Y. Liu, *Toxicol. Sci*., 2017. DOI: 10.1093/toxsci/kfx218.

8 H. He, D. W. Li, L. Y. Yang, L. Fu, X. J. Zhu, W. K. Wong, F. L. Jiang and Y. Liu, *Sci. Rep*., 2015, **5**, 13543.

9 J. Wang, X.-Y. Fan, L.-Y. Yang, H. He, R. Huang, F.-L. Jiang and Y. Liu, *MedChemComm*, 2016, **7**, 2016-2019.

10 K. Rohlenova, K. Sachaphibulkij, J. Stursa, A. Bezawork-Geleta, J. Blecha, B. Endaya, L. Werner, J. Cerny, R. Zobalova, J. Goodwin, T. Spacek, E. Alizadeh Pesdar, B. Yan, M. N. Nguyen, M. Vondrusova, M. Sobol, P. Jezek, P. Hozak, J. Truksa, J. Rohlena, L. F. Dong and J. Neuzil, *Antioxid. Redox Sign.*, 2017, **26**, 84-103.

11 G. Cheng, J. Zielonka, O. Ouari, M. Lopez, D. McAllister, K. Boyle, C. S. Barrios, J. J. Weber, B. D. Johnson, M. Hardy, M. B. Dwinell and B. Kalyanaraman, *Cancer Res.*, 2016, **76**, 3904-3915.

12 J. Rohlena, L.-F. Dong, K. Kluckova, R. Zobalova, J. Goodwin, D. Tilly, J. Stursa, A. Pecinova, A. Philimonenko, P. Hozak, J. Banerjee, M. Ledvina, C. K. Sen, J. Houstek, M. J. Coster and J. Neuzil, *Antioxid. Redox Sign.*, 2011, **15**, 2923-2935.

13 L. Ma, J.-X. Dong, C. Wu, X.-Y. Li, J. Chen, H. Zhang, Y. Liu, *J. Mem. Biol.*, 2017, 250, 195-204.

14 D.-W. Li, H. He, B. Lin, Z.-Q. Xu, F.-L. Jiang, Y. Liu, *RSC Adv.*, 2014, 4, 3913-3919.

15 J. C. Philips, R. Braun, W. Wang, J. Gumbart, E. Tajkhorshid, E. Villa, C. Chipot, R. D. Skeel, L. Kale, K. Schulten, *J. Comput. Chem.*, 2005, 26, 1781-1802.

16 S. J. A. Koh, H. P. Lee, C. Lu, Q.-H. Cheng, *Physic. Rev. B*, 2005, 72, 085414.

17 H. He, J. Xu, D.-Y. Chen, F.-L. Jiang, Y. Liu, *J. Phys. Chem. B*, 2017, 121, 1211-1221.

18 W. Humphrey, A. Dalke, K. Schulten, J. Mol. Graph. Model., 1996, 14, 33-38.

19 W. Zhou, X. Wang, M. Hu, C. Zhu and Z. Guo, *Chem. Sci.*, 2014, **5**, 2761-2770.

20 X. Y. Fan, Y. J. Liu, K. Chen, F. L. Jiang, Y. J. Hu, D. Liu, Y. Liu and Y. S. Ge, *Eur. J. Med. Chem.* 2017. DOI: 10.1016/j.ejmech.2017.05.022

21 D. N. Silachev, L. S. Khailova, V. A. Babenko, M. V. Gulyaev, S. I. Kovalchuk, L. D. Zorova, E. Y. Plotnikov, Y. N. Antonenko and D. B. Zorov, *Biochim. Biophys. Acta - Gen. Sub.*, 2014, **1840**, 3434-3442.

22 J. Li, Y. Zhang, Q. Xiao, F. Tian, X. Liu, R. Li, G. Zhao, F. Jiang and Y. Liu, *J. Hazard. Mater.*, 2011, **194**, 440-444.

23 Y. N. Antonenko, S. S. Denisov, D. N. Silachev, L. S. Khailova, S. S. Jankauskas, T. I. Rokitskaya, T. I. Danilina, E. A. Kotova, G. A. Korshunova,

E. Y. Plotnikov and D. B. Zorov, *Biochim. Biophys. Acta - Gen. Sub.*, 2016, **1860**, 2463-2473.

24 C. Porter, N. M. Hurren, M. V. Cotter, N. Bhattarai, P. T. Reidy, E. L. Dillon, W. J. Durham, D. Tuvdendorj, M. Sheffield-Moore, E. Volpi, L. S. Sidossis, B. B. Rasmussen and E. Borsheim, *Am. J. Physiol. Endoc. M.*, 2015, **309**, E224-232.

25 M. A. Fernandes, J. B. Custodio, M. S. Santos, A. J. Moreno and J. A. Vicente, *Mitochondrion*, 2006, **6**, 176-185.

26 S. S. Denisov, E. A. Kotova, E. Y. Plotnikov, A. A. Tikhonov, D. B. Zorov, G. A. Korshunova and Y. N. Antonenko, *Chem. Commun.*, 2014, **50**, 15366-15369.

27 Y. Jang, S. Kim, W. K. Oh, C. Kim, I. Lee and J. Jang, *Chem. Commun.*, 2014, **50**, 15345-15347.

28 Y. N. Antonenko, S. S. Denisov, L. S. Khailova, P. A. Nazarov, T. Rokitskaya, V. N. Tashlitsky, A. M. Firsov, G. A. Korshunova and E. A. Kotova, *Biochim. Biophys. Acta - Biomembranes*, 2017, **1859**, 377-387.

29 F. Sedlic, A. Sepac, D. Pravdic, A. K. S. Camara, M. Bienengraeber, A. K. Brzezinska, T. Wakatsuki, Z. J. Bosnjak, *Amer. J. Physiol.-Cell Physiol.*, 2010, **299**, 506-515.

30 F. F. Severin, Severina, II, Y. N. Antonenko, T. I. Rokitskaya, D. A. Cherepanov, E. N. Mokhova, M. Y. Vyssokikh, A. V. Pustovidko, O. V. Markova, L. S. Yaguzhinsky, G. A. Korshunova, N. V. Sumbatyan, M. V. Skulachev and V. P. Skulachev, *Proc. Natl. Acad. Sci. USA*, 2010, **107**, 663-668.

31 S. Zhang, *J. Comput. Chem.*, 2012, **33**, 2469-2482.

32 A. Wiederkehr, *Islets*, 2009, **1**, 154-156.

1. We developed two isomers of F16 with totally different fluorescence, uncoupling activity.
2. Isolated mitochondrial were used to investigate the uncoupling efficiency of F16 isomers.
3. Molecular simulations of proton dissociation energy and translocation barrier.